Electrochemical Formation of Germanene: pH 4.5

M. A. Ledina,[a] N. Bui,[a,*] X. Liang,[a] Y. -G. Kim,[b] J. Jung,[a,*] B. Perdue,[a] C. Tsang,[a]
J. Drnec,[c,**] F. Carlà,[c] M. P. Soriaga,[b,**] T. J. Reber,[a] and J. L. Stickney[a,***,z]

[a]*Department of Chemistry, The University of Georgia, Athens, Georgia 30602, USA*
[b]*Joint Center for Artificial Photosynthesis, California Institute of Technology, Pasadena, California 91125, USA*
[c]*ESRF, 38000 Grenoble, France*

Germanene is a single layer allotrope of Ge, with a honeycomb structure similar to graphene. This report concerns the electrochemical formation of germanene in a pH 4.5 solution. The studies were performed using in situ Electrochemical Scanning Tunneling Microscopy (EC-STM), voltammetry, coulometry, surface X-ray diffraction (SXRD) and Raman spectroscopy to study germanene electrodeposition on Au(111) terraces. The deposition of Ge is kinetically slow and stops after 2–3 monolayers. EC-STM revealed a honeycomb (HC) structure with a rhombic unit cell, 0.44 ± 0.02 nm on a side, very close to that predicted for germanene in the literature. Ideally the HC structure is a continuous sheet, with six Ge atoms around each hole. However, only small domains, surrounded by defects, of this structure were observed in this study. The small coherence length and multiple rotations domains made direct observation with surface X-ray diffraction difficult. Raman spectroscopy was used to investigate the multi-layer Ge deposits. A peak near 290 cm^{-1}, predicted to correspond to germanene, was observed on one particular area of the sample, while the rest resembled amorphous germanium. Electrochemical studies of germanene showed limited stability when exposed to oxygen.

Two dimensional (2D) inorganic materials have unique properties that make them attractive for integration into the nanoelectronics industry.[1–3] Ever since the discovery of graphene (a single HC layer of sp^2 carbon atoms), studies of its properties (high intrinsic mobility, large specific area, electrical conductivity, etc.[4]) have indicated tremendous potential for numerous applications, including: nanoelectronics, sensors, batteries, supercapacitors, field-effect transistors, and transparent conductive electrodes.[5–7] Its study has also stimulated researchers into other 2D materials, such as Ge analog of graphene.[8–11] The germanene structure was first calculated in 2009 by Cahangirov et al.[12] It has since been discussed in more than three hundred published papers. The proposed structure of germanene is a 2D hexagonal array of Ge atoms, and van der Waals stacking between the layers. Each layer has a graphene-like (HC) structure. However, unlike the ideally flat sp^2 graphene structure, the energetically stable configuration of germanene is predicted to be low-buckled, with half of the atoms about 0.07 nm above the rest, as a result of some mixed sp^2-sp^3 hybridization (Figure 1).[13] Germanene is a Dirac 2D material despite its buckled structure.[14] Its bandgap is thus larger than graphene, about 24 meV, making germanene semimetallic.[15–17] The Ge-Ge nearest neighbor distance is 0.24 nm, resulting in 0.41 nm between 6 membered rings (Figure 1).[18] A Raman shift of about 290 cm^{-1} has been predicted from ab initio studies.[19–24]

Germanene appears to be a unique material that does not exist in nature. However, due to the possibility of germanene being more facilely integrated into Si nanotechnology than graphene,[16,25] development of synthetic methods for its formation are of interest. The silicon version of graphene, silicene, is generally unstable outside vacuum.

The deposition of germanene on metal surfaces in vacuum has been previously reported. On Pt(111), a $(\sqrt{19} \times \sqrt{19})$R23.4° buckled structure has been synthesized in UHV by electron beam physical vapor deposition at room temperature, with subsequent annealing. According to STM images, and ab initio calculations, it was concluded that only one atom was higher in the six-member Ge atoms hexagon structure.[26] In another report a $(\sqrt{3} \times \sqrt{3})$R30° germanene layer was formed on a $(\sqrt{7} \times \sqrt{7})$R19.1° Au(111) supercell, deposited

by molecular beam epitaxy (MBE). The observed STM images displayed a honeycomb-like structure, though it was found to be nearly flat with interatomic distances of 0.255 nm.[27] Moreover, the same investigators reported formation of a few layers thick germanene structures with the same atomic distances (0.256 nm) and steps heights of about 0.32 nm.[28] A (3×3) superstructure with similar interatomic distances was also observed on Al(111). The height of the germanene layer was found to be about 0.27 nm.[18] Formation of a germanene structure was also reported after evaporation of Pt onto Ge(110) and consequent flash annealing.[29] Furthermore, multi-layered germanene (lonsdaleite germanium) was synthesized on a Si substrate by first depositing epitaxial Si$_{0.65}$Ge$_{0.35}$, and then exposure of the sample to a N$_2$
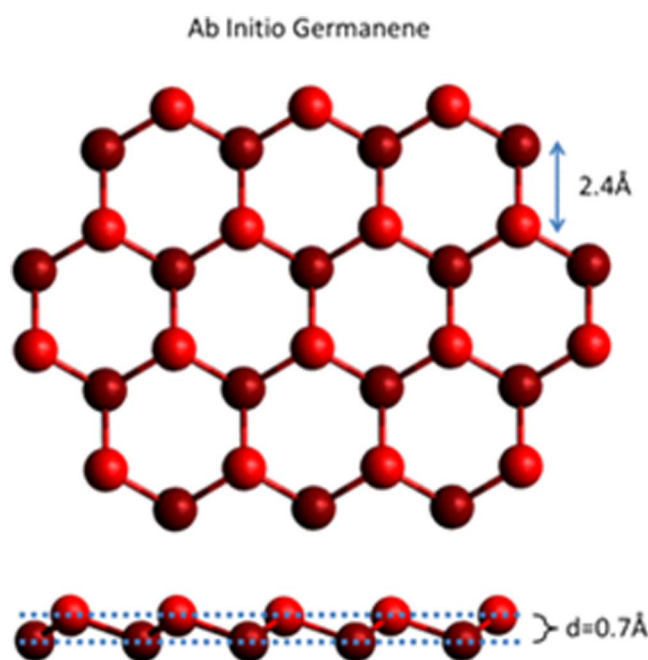

Figure 1. Proposed low-buckled germanene structure. One half of the Ge atoms are 0.07 nm higher than the other half.

plasma and sequential annealing.[30] D'Acapito et al. reported an X-ray absorption spectroscopy (XAS) study on the formation of Ge layers by MBE on an AlN buffered Ag substrates. First-principles calculations and the experimental data suggested the formation of germanene with atomic distances of 0.238 nm.[31] In addition, layered germanane, the hydrogenated form of germanene, was obtained through a topotactic deintercalation of $CaGe_2$.[32]

Due to its low hydrogen overpotential and the limited reactivity of Ge ions, electrodeposition studies of germanium were mostly performed in nonaqueous media.[33–37] For example, Szekely has reported formation of Ge films by electrodeposition from a solution of germanium tetrachloride in propylene glycol with a plating speed of 0.001 in./3 hr.[34] Endres et al. have published a number of contributions concerning Ge electrodeposition studies from molten salts and ionic liquids, and was the first to use in situ STM for this system.[38–42] Using germanium tetraiodide as a precursor resulted in a maximum deposit thickness of 20 nm.[38] Cyclic voltammetry studies by different researchers in nonaqueous media suggest that the deposition involved reduction of a Ge^{+4} species to a Ge^{+2} species, and subsequent reduction to $Ge°$.[36,41–46] Ge electroplating has also been reported on semiconducting substrates such as Si.[47] There are some reports on the formation of thick Ge nanostructures,[48–50] which showed that, depending on potential, Ge nanostructures can be grown from aqueous solution by dissolution into and saturation of a liquid Hg electrode.[50] Ge nanowires were also formed by Al-Salman et al. by utilizing a solution of Ge in ionic liquids.[44] Bartlett et al. have studied electrodeposition of Ge from various supercritical fluids containing Ge(II) or Ge(IV) compounds.[46] They were able to obtain amorphous Ge films from Ge(IV) and Ge(II) precursors; however, films grown from Ge(II) compounds were heavily contaminated.

The authors have been investigating Ge electrodeposition from aqueous solutions onto Au and Cu substrates.[51–53] The direct electrodeposition of Ge at a controlled potential from aqueous media appeared to be limited to 2–4 monolayers (ML), where a ML is defined here as one adsorbate atom per substrate surface atom. Still less Ge was observed depending on the potential, time and the pH used. To increase Ge coverages, an electrochemical ALD cycle (E-ALD) was developed, making use of surface limited reactions to grow Ge films an atomic layer at a time per cycle. That cycle was repeated to grow thicker deposits. At that time, Raman spectroscopy indicated formation of amorphous Ge, from a broad peak at 270 cm^{-1}.[53]

As mentioned above, germanene formation has been reported using gas-phase synthetic methods, requiring ultrahigh vacuum and elevated temperatures/annealing. The present report discusses investigations into the electrochemical formation of germanene layers on an Au electrode in pH 4.5 aqueous solutions. Those deposits were studied at room temperature using EC-STM, cyclic voltammetry, micro-Raman spectroscopy and SXRD.

Experimental

EC-STM studies were performed using a Nanoscope III (Digital Instruments). All images were obtained in constant current mode. Electrochemical studies were performed using a three-electrode configuration, with an Ag/AgCl (3 M NaCl, BASI) reference, a platinum wire auxiliary, and an Au bead working electrode. Imaging was performed on Au(111) facets of a bead, prepared using a variation of the Clavilier method.[54] Before each experiment, the Au bead was flame annealed, cooled down in a hydrogen atmosphere and quenched in ultrapure water (>18.2 MΩ) saturated with hydrogen, to ensure cleanliness and formation of large (111) terraces. The bead was quickly inserted into the EC-STM cell to avoid contaminations. 300–500 nm terraces were typically observed. STM tips were 0.25 mm tungsten rods, electrochemically etched in 1 M KOH solution, at 15 V ac, just prior to use. The tips were then coated with nail polish to reduce solution contact area, and thus faradaic reactions, leaving only the tip apex uncovered. The tip potential, E_t, was generally near −150 mV vs. Ag/AgCl. The STM was calibrated using HOPG. All glassware and parts were cleaned daily.

Aside from EC-STM studies, other electrochemical studies were performed using an automated electrochemical flow cell deposition system (Electrochemical ALD L.C., Athens, GA). The E-ALD hardware consisted of a flow cell, solenoid valves, solution reservoirs, pumps, relay box and potentiostat, all controlled using specialized "Sequencer 4" software. Solution reservoirs were purged with nitrogen, and valves and tubing were confined in a nitrogen atmosphere. The flow cell was also of a three-electrode configuration. The working electrodes (substrates) were 100 nm thick polycrystalline Au films, vapor deposited on a 5 nm thick Ti film on glass. The reference was an Ag/AgCl (3 M NaCl, BASI, West Lafayette, IN), and the auxiliary was an Au wire inlayed into the face of the flow cell, parallel to the substrate in order to simplify the current distribution. Each Au substrate was cleaned by cycling in 0.1 M sulfuric acid before use.

The SXRD measurements were performed at ID03 beamline at ESRF, France. The incident beam (E = 24 keV) was focused to 50×300 μm (vertical × horizontal) relative to the plane of the surface. The electrochemical setup consisted of a three-electrode-PEKK flow cell,[55] a PAR263 potentiostat and an automatic electrolyte distribution system. All glassware, teflon tubing and the PEEK cell were cleaned either in hot sulfuric acid or in diluted piranha solution prior to the experiment. The raw data were reduced to the rod profiles using BINoculars[56] according to a previously described procedure.[57] The fits were performed with the ROD code.[58]

All solutions were prepared with reagent grade chemicals and ultrapure water (18 MΩ, obtained from a Millipore-Q system, fed with in-house DI water). Blank and germanium solutions contained 0.1 M or 0.05 M $KClO_4$ (Aldrich, 99.99% trace metals basis). The germanium solutions also contained 1 mM GeO_2 (Alfa Aesar, 99.999%, metals basis) in addition to the electrolyte. The solutions were pH 4.2 – 4.7, though no buffer was present. Raman spectra were obtained using a Renishaw InVia Raman microscope (Renishaw, Inc., Hoffman Estates, IL) with a 514 nm laser.

Results and Discussion

Figure 2 displays Ge deposition and stripping cyclic voltammetry (CV) on polycrystalline Au on glass, from a pH 4.5 germanium oxide (GeO_2) solution. The potential was scanned from 500 mV to increasingly negative potential limits, and back. It suggests that Ge deposition starts near −550 mV, and displays a peak at −1250 mV.

The oxidation process appears totally irreversible, given that it all occurs positive of −550 mV (Figure 2), that the reduction charge is

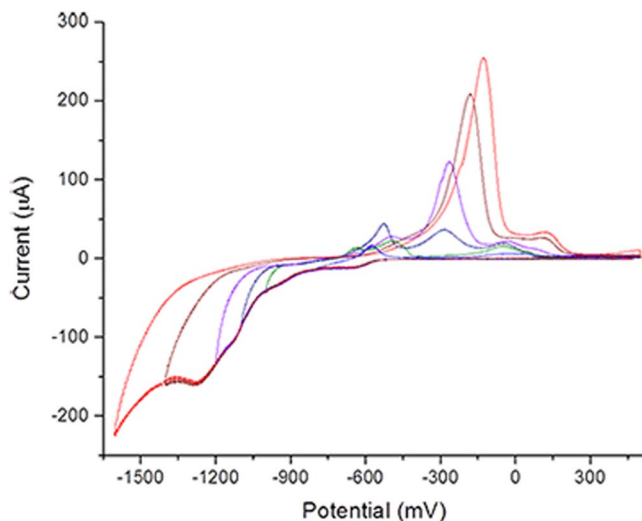**Figure 2.** Window opening CVs of 0.5 mM GeO_2, 0.1 M $NaClO_4$ (pH 4.5) on a polycrystalline Au substrate from cathodic limits of −700 mV to −1600 mV while the anodic limit was kept to 500 mV for each cycle. The scan rate used was 10 mV/s. Area = 2 cm^2.
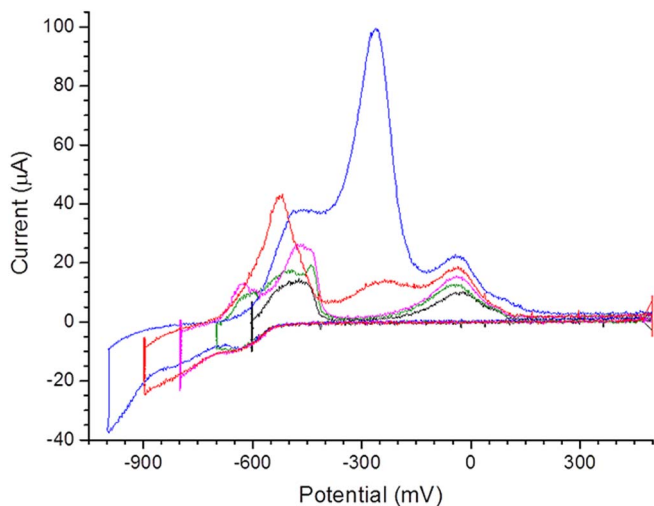
Figure 3. Window opening CVs of 0.5 mM GeO$_2$, 0.1 M NaClO$_4$ (pH 4.5) on a polycrystalline Au substrate from cathodic limits of −600 mV to −1000 mV, holding at these potentials for 700 sec, while the anodic limit was kept to 500 mV for each cycle. The scan rate used was 10 mV/s. Area = 2 cm^2.

Figure 5. STM image of Au(111) herringbone (HB) reconstruction in 1 mM GeO$_2$ and 0.1 M KClO$_4$ (pH 4.2) before Ge deposition, at −300 mV vs. Ag/AgCl.

more than twice that for the oxidation suggests H$_2$ formation during deposition. Some of the evident irreversibility results from changes in surface pH. That is, as H$_2$ forms, the pH at the surface increases, shifting Ge deposition negatively. For comparison, Figure 3 displays a series of CVs where the potential was held at the negative limit for 700 s, helping to complete deposition and stabilize the surface pH. Note that the purple Ge oxidative stripping curve in Figure 2, where the potential was reversed at −1200 mV, was obtained in Figure 3 (blue) after holding at only −1000 mV, for 700 s.

Time dependent studies showed that small quantity of Ge can be deposited at potentials positive of −550 mV, if the potential was held for a sufficient time (Figure 4). If the potential was not held at −500 mV (red CV), the oxidation scan gives no indication of Ge oxidation stripping. However, Ge oxidation is evident if the potential was held at the negative limit (200 s blue, 500 s black, and 700 s green). The
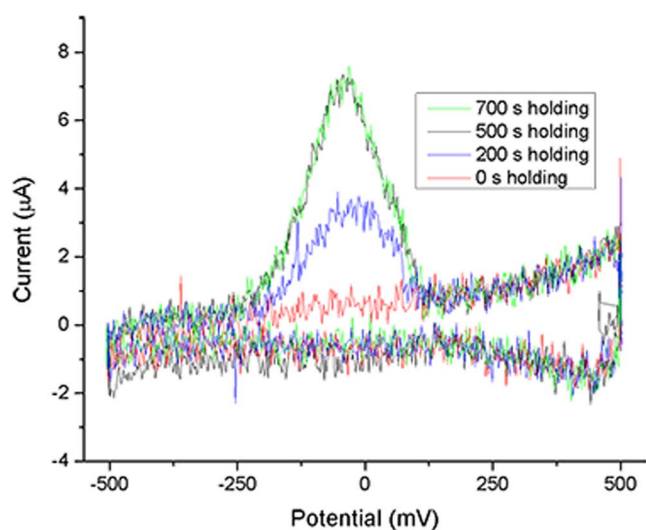
same profiles of black and green curves indicate a saturated 0.1 ML Ge coverage at −500 mV.

Figure 5 is an in situ EC-STM image of the ($\sqrt{3} \times 22$) herringbone (HB) Au(111) reconstruction, recorded at −300 mV in the GeO$_2$ solution. The image appears equivalent to those previously observed for clean Au(111) surfaces in solution, in the absence of Ge. On the other hand, at −600 mV the STM images in Figure 6 were obtained, where Ge coverage near 0.2 ML was deposited while the surface reconstruction took place (Figure 3, black). The surface (Figure 6) displays a disordered reconstruction, with excessive elbows and rotations in the ridges, as well as pits at some of the elbows. It turns out that the potential for reconstruction of the Au(111) surface to the HB is about −300 mV, while Ge appears to begin depositing near −400 mV. The surface in Figure 6 resulted from a step to −600 mV, so both the reconstruction and the beginning of Ge deposition took place together, possibly accounting for the disorder in the reconstruction. The defects in the surface, such as the holes (Figure 6b) and the wider areas between ridges, appear to be associated with Ge nucleation.

To check further the structure of the reconstruction after fast Ge deposition, SXRD measurements were performed on the reconstructed surface and after deposition of ≈0.1 ML. The HB reconstruction was first formed at −500 mV (Figure 7a) and the subsequent measurements were taken at this potential. The reconstruction shows itself in the SXRD as set of four reconstruction rods positioned around the (1,0) crystal truncation rod (CTR) as seen in the in-plane cut of reciprocal space (Figure 7a).[59] The measurement of the specular (0,0) CTR (Figure 7c) confirms the low roughness of the surface and

Figure 4. Oxidative stripping scans in 0.5 mM GeO$_2$, 0.1 M NaClO$_4$ (pH 4.7) on a polycrystalline Au substrate, after scanning to −500 mV from 500 mV and holding the potential for 0, 200, 500, or 700 s. The scan was performed at 10 mV/s, without solution flowing in the electrochemical flow cell. Area = 2 cm^2. Assuming a 4 e$^-$ process, the oxidation peak at −50 mV indicated the presences of 0.062 ML of Ge after 700 s & 500 s, and 0.036 ML of Ge after 200 s.
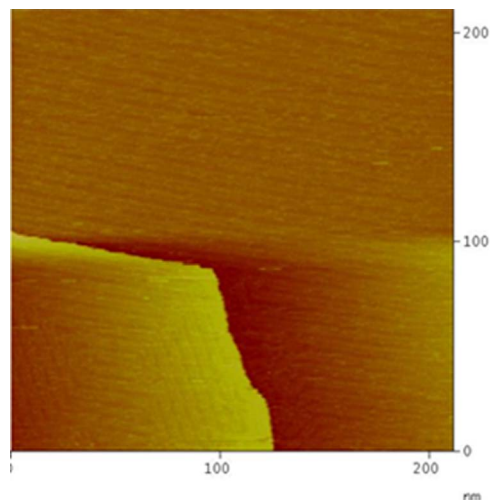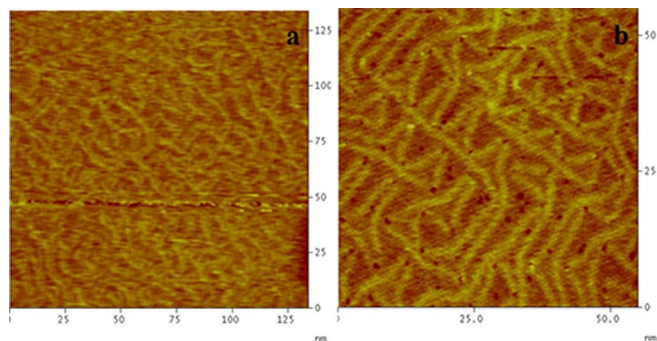

Figure 6. STM image of Au(111) in 1 mM GeO$_2$ and 0.1 M KClO$_4$ (pH 4.2). Potential was stepped from −300 mV to −600 mV vs. Ag/AgCl in Ge solution. HB lines restructured to a new pattern due to adsorption of Ge onto the surface.
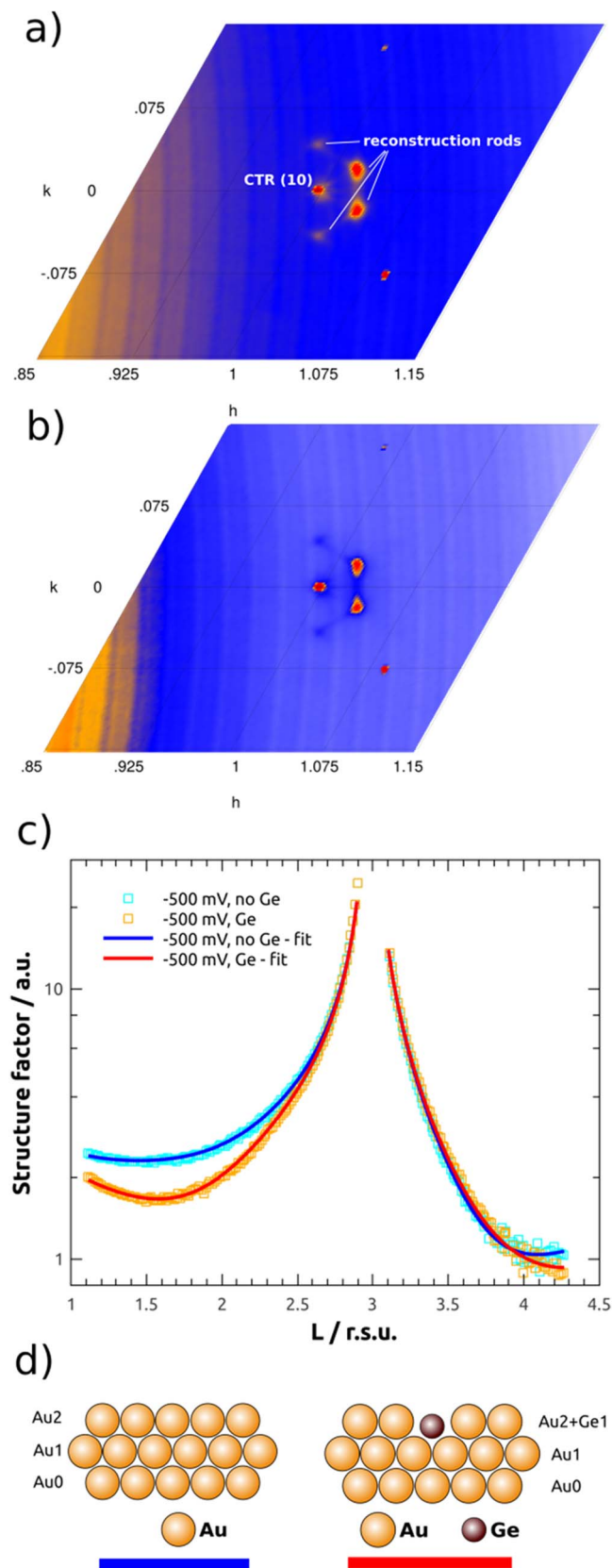
Table I. Paramaters of the models used to fit the SXRD data showed in Figure 7c and 7d. x is an occupancy parameter, d is a distance between different surface planes as noted in Figure 7d, DW is a Debye-Waller parameter and norm χ^2 is normalized chi squared.

	−500 mV, no Ge	−500 mV, Ge
x_{Au1}	0.973 ± 0.005	0.97 ± 0.02
x_{Au2}	1.03 ± 0.01	0.89 ± 0.13
x_{Ge1}		0.07 ± 0.09
$d_{Au1-Au2}$	2.446 ± 0.005	2.41 ± 0.02
$d_{Au1-Ge1}$		1.2 ± 2.6
DW_{Au2}	3.5 ± 0.1	2.2 ± 0.8
DW_{Au1}	0.7 ± 0.1	0.8 ± 0.1
DW_{Ge1}		0 ± 44
Norm χ^2	0.88	0.95

generally good quality of the reconstruction. The important fitting parameters are shown in Table I. The top reconstructed layer is slightly relaxed outwards by 3.8% compared to the bulk interlayer distance, which correspond well with the value obtained previously with the same technique in vacuum (3.3%).[60] The fits also indicate 6% higher atomic density in the topmost layer compared to the bulk as expected for the compressed HB reconstruction.

While the potential was kept at −500 mV, the electrolyte was changed to Ge containing electrolyte and the SXRD measurements were repeated. There are some noticeable differences: the minimum of the (0,0) CTR shifts downward signaling Ge deposition and the in-plane cut of the reciprocal space map shows that the reconstruction was maintained but the reconstruction rods appear to be weaker, supporting the STM observation of increased reconstruction disorder upon Ge deposition (Figure 7b). From the (0,0) CTR fitting, we can determine the out-of-plane position of deposited Ge. Two models were proposed: i) Ge is incorporated in the reconstruction and ii) Ge is located on top of the reconstructed surface. In both cases the Ge coverage was similar, ≈0.07 ML for the incorporated Ge incorporation and ≈0.08 ML for the on-top Ge. However, better fit was obtained with the Ge incorporation model as judged from the normalized χ^2 values (Table I). In this model the Au surface atoms belonging to the HB reconstruction are replaced by the adsorbed Ge (Figure 7d). The outward relaxation of the topmost Au atoms is slightly decreased while Ge atoms are positioned closer to the underlying Au layer as expected from the smaller size of Ge. Notably, the errors related to the Ge position, coverage and DW are large pointing to the high uncertainty in the location of the incorporated Ge atoms.

Similar behavior of the HB reconstruction during the deposition is reported in the literature.[61–63] For example, Nahas et al. reported such behavior after deposition of Pt onto Au(111).[62] They suggested that random intrusion of Pt atoms into the surface caused reconstruction modifications. In this case Ge atoms might incorporate at the elbows due to the edge dislocations present on the reconstructed surfaces, creating preferred binding spots.[64,65] Sun et al.[66] also observed similar behavior for the reconstruction after adsorption of a monolayer of perylene (FePc).

The image in Figure 8a shows results from an experiment where the HB was first formed at −300 mV and then the potential was slowly shifted to −400 mV, where small amount of Ge can be deposited (Figure 4). This can be compared to Figure 6, where the potential was stepped directly to −600 mV. Figure 8a shows 5–10 nm-long lines on the surface, which increased in number slowly while the potential was held at −400 mV. The STM tip had some influence on the positions of the lines, and may have influenced line growth as well. Lines also grew on areas which had not been imaged, suggesting the STM tip was more a small perturbation than a method of line synthesis. Close inspection of sequential images indicated that the lines moved short distances and slowly grew in length, depending on the potential. It was also observed that the HB was present under the lines. Reconstructions can be lifted by adsorption. That the lines did not lift the HB suggests

Figure 7. a) In-plane reciprocal space map of a HB reconstruction formed at −500 mV in 0.1 M KClO$_4$ (pH 4.2). b) In-plane reciprocal space map after deposition of about 0.1 ML of Ge at −500 mV vs Ag/AgCl in 1 mM GeO$_2$ and 0.1 M KClO$_4$ (pH 4.2) showing maintained HB reconstruction. c) The profile of specular (0,0) CTR before and after Ge deposition at −500 mV. The solid lines correspond to the fit of the models shown in d).
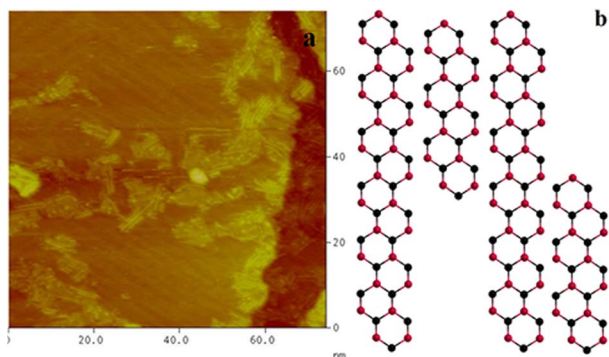
Figure 8. a) STM image of Au(111) in 1 mM GeO$_2$ and 0.1 M KClO$_4$ (pH 4.2) at -400 mV vs. Ag/AgCl, showing germanene nanoribbons on the Au herringbone reconstruction. a) Formation of germanene nanoribbons at -400 mV lingering on top of the Au herringbone reconstruction. b) Proposed structures for germanene ribbons.

that the Ge interacted only weakly with the Au surface, as expected for van der Waals bonding.

Measurements of line heights varied between 0.1 nm and 0.06 nm, with all measurements less than expected for an atomic layer. The lines might be atoms partially buried in the surface; however, they would be expected to strongly interfere with the reconstruction and not be expected to move significantly between images. If these thin lines are not strongly bound to the surface they should be influenced by imaging, which would account for their small movements and the difficulties determining their heights. Alternatively, the tunneling conditions, work function, may be very different between the Au HB and the lines. The inter-line spacing varied, but was generally near 0.8 nm to 1 nm.

It is proposed here that the lines might be thin ribbons of germanene weakly adsorbed on top of the underlying Au(111) HB. Figure 8b is a diagram of a nanoribbon structure, based on dimensions from Figure 1.[13,15,18] Related ribbon structures have been observed by other authors concerned with silicene, the silicon analog of graphene and germanene.[67–74] The ribbons appear near step edges, both above and below, and near defects or disordered sites in the reconstruction. In addition to the gradual appearance of the ribbons in Figure 8a, a small number of 0.2 nm high islands were also observed, and appear to be single atom high Au(111) islands coated with the germanene ribbons. The Au(111) islands probably result from atoms released by relaxation of the HB.[75]

Figure 9a shows an image of the disordered reconstructed surface at -600 mV, which has a Ge coverage of 0.2 ML as determined from coulometry. Figure 9b shows a subsequent image where the potential was stepped from -600 mV to -700 mV half way up the scan, the bottom half was taken at -600 mV and the top half at -700 mV with the evident spray of particles. The particles appear to be similar in dimensions to the ribbons described above, each a few nm in size. Figure 9c was the subsequent down scan, in which most of the particles disappeared from the image. In addition, 8c displayed one atom deep horizontal pits of unknown origin across the image, though no conditions were changed between 8b and 8c. In Figure 9d the scanned area was enlarged, from 170 nm to 300 nm, and piles of the particles were evident on the left and right sides of the previous scanned area (Figures 9a–9c), suggesting they were not strongly bound to the surface and the tunneling conditions swept them from the field of view. These Ge nanoparticles were molecular in size, probably small pieces of the germanene, similar to the ribbons. They formed in Figure 9b in a couple of seconds, after stepping to -700 mV, possibly facilitated by Ge accumulated at or in the Au surface while holding at -600 mV.

The above experiments point to the fact that the preparation procedure plays a crucial role in the Ge deposition. Both on-top Ge (germanene) and incorporated Ge or both can be formed depending on the exact potential control sequence.
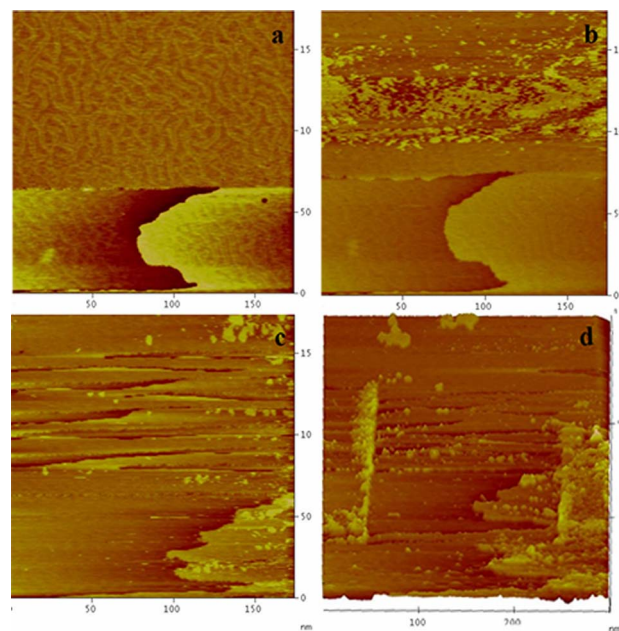

Figure 9. STM images of Au(111) in 1 mM GeO$_2$ and 0.1 M KClO$_4$ (pH 4.2) taken 30 s apart. a) at -600 mV vs. Ag/AgCl; b) after the potential was stepped to -700 mV; c) no change in conditions; d) no conditions were changed, however the scan area was expanded to show the piles of Ge.

After holding at -800 mV, Figure 3 (pink), there are two oxidation features, at -500 mV and -50 mV. The peak at -50 mV is nearly constant in each scan and accounts for stripping of the last Ge from the Au surface (about 0.2 ML) and it is referred here as oxidation of the underpotentially deposited Ge (UPD).[38,76,77] UPD describes the electrodeposition of an atomic layer of one element on a second, the substrate, in a surface limited reaction. The other oxidation feature, between -400 mV and -700 mV, is more easily oxidizable Ge, arguably the result of oxidation of molecular scale germanene flakes from their edges. The low potential stripping peak was present in Figure 3 where the potential was held at -600 (black), -700 (green) or -800 mV (pink). Between the low potential and high potential stripping peak, however, is essentially no oxidative current passed. On the other hand, holding at -900 mV (red), or below (blue), an oxidation peak near -300 mV grows. The current in the new peak near -300 mV increased as the potential was held at more negative limits and for longer times, until the peak area saturated at 2 to 3 ML. Figure 2 displayed the same behavior, though the potential was not held, but simply reversed at increasingly negative limits. Note that in addition to the maximum current, potential increases with the more negative the potential limit, and the peak between -700 mV and -400 mV becomes suppressed as the -300 mV peak grows.

A pH dependence to the Ge coverage had previously been shown, with pH 9 resulting in slightly more than pH 4.5.[52] Ge coverages were determined using coulometry: integration of the currents recorded during oxidative Ge stripping (Figures 2 and 3), with the assumption here that the GeO$_2$ in solution existed as H$_2$GeO$_3$ and underwent a 4 e$^-$ reduction to Ge^0 on the surface. XPS studies, by this group, indicated elemental Ge was present after deposition at the more negative potentials.

Figure 10 shows in situ STM images of an Au(111) facet on the Au bead electrode after scanning to -1400 mV and then back to -900 mV, where the potential was held during imaging. At -1400 mV, hydrogen evolution was extensive making imaging difficult, while at -900 mV the hydrogen evolution was minimized and the deposits remained stable enough to be imaged. Images in Figure 10 revealed the honeycomb nature of the Ge deposits, although the domains were small and only coherent in a nm scale. Based on the STM and coulometry from stripping of saturated Ge deposits, it was concluded that the
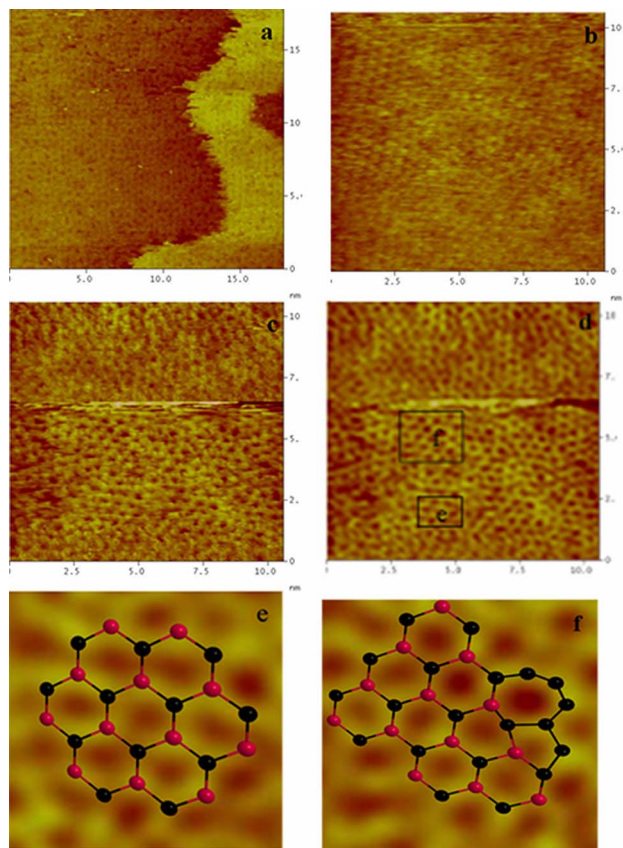
Figure 10. a-f are STM images of Au(111) in 1 mM GeO$_2$ and 0.1 M KClO$_4$ (pH 4.2) after the potential was scanned to −1.4 V and then to −900 mV vs. Ag/AgCl. a) shows a strip of germanene on a layer of germanene. b) shows honeycomb structure, with 0.44 ± 0.02 nm between the holes. c) shows nearly atomically resolved germanene. Image d is FFT processed image c to enhance honeycomb structure. The boxes indicate where figures e and f were taken. e) Superposition of honeycomb structure drawing on FFT of germanene domain STM image. f) Superposition of germanene drawing, including 5- and 7-membered rings at domain wall, on FFT of germanene STM image.

Au surface was coated with the equivalent of two to three monolayers of Ge.

Figure 10a is an image of a strip of germanene on a germanene layer. The height of the strip was 0.35 nm above the underlying germanene, consistent with van der Waals bonding. The expected distance hole-to-hole in the honeycomb structure of germanene (Figure 1) is 0.41 nm, while the distance measured on Figure 10b is 0.44 ± 0.02 nm which is close to the expected value.[18]

Figure 10c is a nearly atomically resolved image of a germanene deposit, showing the small coherent HC regions surrounded by different sized rings and rotated domains. Figure 10d is Figure 10c after a Fast Fourier Transform (FFT) filter, which removed any atomic resolution, accentuated the HC periodicities, the variation in hole size, the short coherence lengths and the angles between lines of holes in the HC domains. The short coherence lengths resulted from changes in bonding at domain walls, and are highlighted by variation in ring size (Figure 10e). Instead of only 6-atom rings, 5- or 7-atom rings were also present (Figure 10f), resulting in rotations of adjacent HC domains. The rectangles in Figure 10d indicate the regions where Figures 10e and 10f were taken. Studies of defects in graphene indicate that atom ejection lead to a recombination of the surrounding atoms to the rings with other than 6 atoms.[78–81] The most common combinations were 5-7-7-5 and 5-8-5 rings, however, the average number of atoms per ring was still 6.[80] Figure 10d reveal cluster defects of this type. A second type of defect results from change of the buckling structure. Ideally, the heights of the atoms alternate (Figure 1). How-

ever, other configurations might also be feasible as they are expected to be only slightly higher in energy. For instance, neighboring atoms in a 6-membered ring might be both positioned higher, which would result in a small localized puckering in the low-buckle HC structure.

The authors suggest the defects in the germanene HC structure resulted from the growth mechanism. That is, it is believed that pieces of molecular germanene were nucleated first at some step edges or defects on the Au(111) substrate. Growth then continued at the edges until they made contact and grew together. The nanoparticles bonded when they encounter each other, but only in small domains of the HC structure. This growth does not appear to be reversible, under the conditions used, leading to the extensive amount of defects evident in Figure 10. The van der Waals nature of the germanene provides flexibility to the growth process, given the limited templating from lattice matching with the substrate.

The SXRD measurement confirms the formation of germanene layer (Figure 11 and Table II). The in-plane map of germanene layer
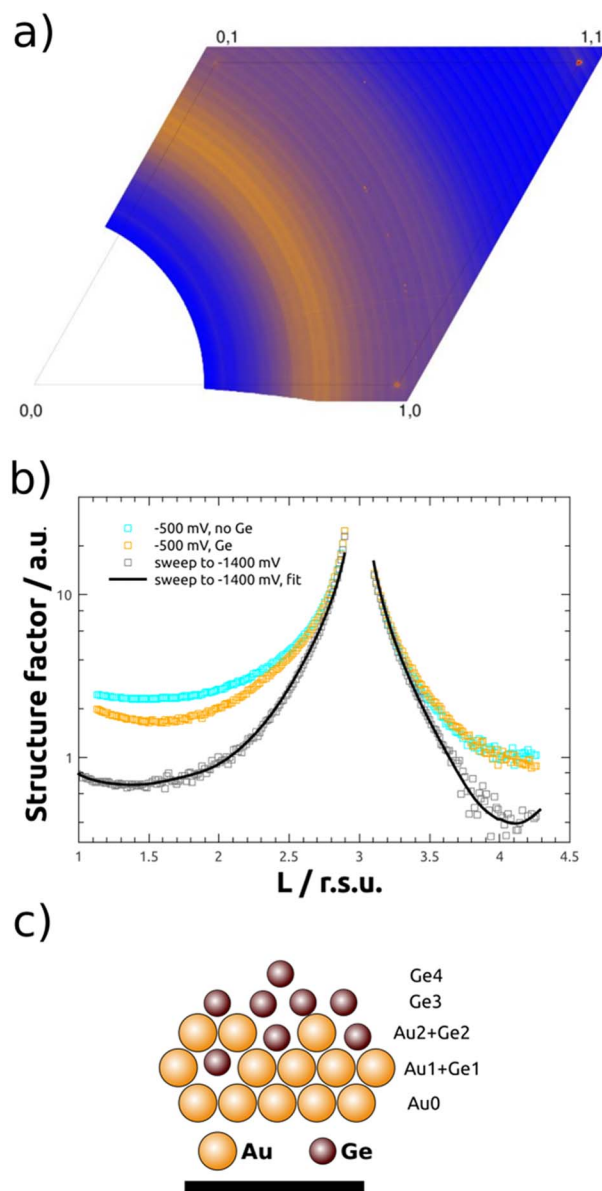

Figure 11. a) In-plane reciprocal space map of a Ge layer formed after the potential was swept to −1400 mV and back to −900 mV vs Ag/AgCl in 1 mM GeO$_2$ and 0.1 M KClO$_4$ (pH 4.2). b) The profile of specular (0,0) CTR of the Ge layer deposited in a). The solid lines correspond to the fit of the models shown in c).

Table II. Paramaters of the models used to fit the SXRD data showed in Figure 11b and 11c. x is an occupancy parameter, d is a distance between different surface planes as noted in Figure 11d, DW is a Debye-Waller parameter and norm χ^2 is normalized chi squared.

	After sweep to -1400 mV and back to -900 mV
x_{Au1}	0.90 ± 0.14
x_{Au2}	0.6 ± 1
x_{Ge1}	0.06 ± 0.1
x_{Ge2}	0.3 ± 1
x_{Ge3}	0.39 ± 0.06
x_{Ge4}	0.17 ± 0.02
$d_{Au1-Au0}$	2.33 ± 0.01
$d_{Au2-Au1}$	2.4 ± 0.2
$d_{Ge1-Au0}$	3 ± 1
$d_{Ge2-Au1}$	3 ± 1
$d_{Ge3-Au2}$	2.6 ± 0.3
$d_{Ge4-Ge3}$	2.56 ± 0.06
DW_{Au1}	2.8 ± 0.1
DW_{Au2}	7 ± 5
DW_{Ge1}	10 ± 30
DW_{Ge2}	10 ± 30
DW_{Ge3}	0 ± 3
DW_{Ge4}	0 ± 3
Norm χ^2	2.63

Figure 12. Raman spectra of Ge wafer (black) with a sharp peak near 300 cm^{-1}, germanene spot (red) close to 290 cm^{-1}, obtained from E-ALD Ge deposit,[51] and amorphous Ge (blue) at 270 cm^{-1}. The 290 cm^{-1} band was observed in a very limited area of the sample.

deposited by the same potential sequence as in the STM measurements show no reconstruction of the underlying Au(111) substrate. Therefore the reconstruction have been lifted due to the Ge deposition. This is unexpected given the weak interaction of germanene with the substrate. To further probe the out-of-plane structure of the formed layer, we fitted the specular (0,0) CTR (Figure 11b) with a model showed in Figure 11c). Three models with different Ge position were tried: i) Ge only on top of the substrate, ii) Ge alloyed within the substrate and (iii) combination of both above cases. The model where part of Ge is alloyed within the substrate and part resides gave the best fit as determined from the normalized χ^2 and the F-test. This is not surprising as the incorporation of the deposited Ge atoms was observed at the onset of deposition as well. The parameters of the best fitting model are shown in Table II. In this model about 0.4 ML of Ge is incorporated in the substrate in two layers. This coverage is, however, associated with a large error highlighting the uncertainty of the alloy structure. For the same reason all parameter errors associated with Ge1 and Ge2 are large. On top of this alloy are two germanene layers with occupancies 0.4 ML and 0.2 ML. This is less then expected most due to the inhomogeneous nature of the Ge layer. The distance of the germanene layer from the substrate was determined to be ≈2.6 Å, lower then the distance determined from STM measurement. This measurement suggest that the layer is a mix of a germanene and more tightly bonded Ge structure. It is also likely that the local structure of the underlying alloy plays a role.

Thicker films of Ge were previously formed using a form of electrochemical atomic layer deposition (E-ALD).[51–53] Raman spectra of the resulting deposits[53] indicated the presences of amorphous Ge. However, one sample examined using micro-Raman spectroscopy, Figure 12, produced a number of spectra from a particular area which displayed a band near 290 cm^{-1}. The peak close to 300 cm^{-1}, Figure 12, was obtained from a Ge(100) wafer. According to published reports, a peak near 290 cm^{-1} corresponds to a "G-like" shift in the germanene layer.[22,24] Moreover, Maldonado et al. studied Ge electrodeposition onto a surface enhanced Raman substrate (SERS-active Au) on which the self-limited amount of Ge had been deposited. In that study a peak at 290 cm^{-1}, at -1.2 V in a pH 9.2 Ge solution, was observed. Although germanene was not mentioned in that article, the results here suggest that it was formed.[82]
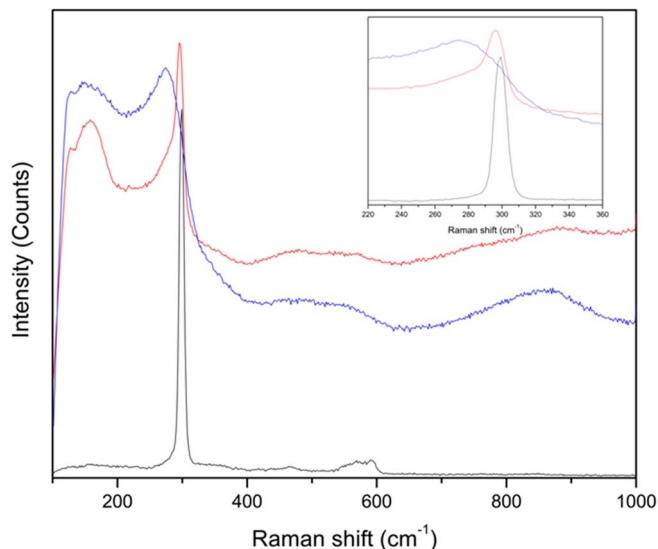
Conclusions

Electrochemical deposition of Ge onto Au and the formation of germanene in aqueous media have been discussed. Initial Ge deposits near -400 mV resulted in fractions of a Ge ML. At longer times at -400 mV, ribbons of germanene were observed near step edges and defects in the HB Au(111) surface. At more negative potentials, -600 mV or -700 mV, extensive disordering of the HB was observed, and correlated with Ge incorporation on the Au surface. Below -700 mV, germanene domains began to form between the patches of the HB. Those domains grew with time, slowly replacing the HB with germanene. At the same time, small Au islands appeared, probably the result of Au atoms released with the loss of the HB. The result was formation of a layer of germanene on the surface, which was followed by growth of large number of small islands of germanene, as a second layer of germanene was formed.

Depending on the potential-time program, STM and voltammetry suggest that nanoclusters of germanene were formed which were not strongly held to the surface, and were swept aside under the tunneling conditions. From voltammetry, the nanoparticles were easily oxidized during the positive scan. As larger sheets of germanene are formed, oxidation become less reversible and a new oxidation peak at around -300 mV began to grow in, shifting positive with increasing germanene coverage. It is proposed that this peak corresponds to a slower process, where the sheets oxidize at the edges, working in.

Images of the honeycomb-like structure of germanene obtained at potentials negative of -1000 mV, where the hole-to-hole spacing was found to be 0.44 ± 0.02 nm. Although freestanding sheet of germanene is predicted to have an interatomic distance of 0.24 nm, germanene grown on Au showed a Ge-Ge distance of 0.255–0.256 nm.[27,28] These numbers suggested a slight enlargement of the spacing between holes, from 0.41 to 0.44 nm, which neatly coincides with the measurement obtained from this study. However, as can be seen from the images, the coherence lengths in domains of germanene were small. The domain walls appear to be composed of 5- or 7-atom rings, instead of the ideal 6. The walls result in small rotations between adjacent domains. The SXRD measurements also confirmed formation of germanene layer after similar conditions to STM ones were used.

Micro-Raman spectroscopy of a thicker Ge deposit, previously made using an E-ALD cycle referred to as "Bait and Switch", was performed. A Raman peak near 290 cm^{-1} was observed, consistent with a predicted peak for germanene.

References

1. A. Dimoulas, "Silicene and germanene: Silicon and germanium in the "flatland"," *Microelectron Eng*, **131**, 68 (2015).
2. S. Balendhran, S. Walia, H. Nili, S. Sriram, and M. Bhaskaran, "Elemental Analogues of Graphene: Silicene, Germanene, Stanene, and Phosphorene," *Small*, **11**(6), 640 (2015).
3. S. Kaneko, H. Tsuchiya, Y. Kamakura, N. Mori, and M. Ogawa, "Theoretical performance estimation of silicene, germanene, and graphene nanoribbon field-effect transistors under ballistic transport," *Appl. Phys. Express*, **7**(3), 035102/1 (2014).
4. Y. Zhu, S. Murali, W. Cai, X. Li, J. W. Suk, J. R. Potts, and R. S. Ruoff, "Graphene and Graphene Oxide: Synthesis, Properties, and Applications," *Adv. Mater. (Weinheim, Ger.)*, **22**(35), 3906 (2010).
5. K. S. Novoselov, A. K. Geim, S. V. Morozov, D. Jiang, Y. Zhang, S. V. Dubonos, I. V. Grigorieva, and A. A. Firsov, "Electric Field Effect in Atomically Thin Carbon Films," *Science (Washington, DC, U. S.)*, **306**(5696), 666 (2004).
6. X. Li, Y. Zhu, W. Cai, M. Borysiak, B. Han, D. Chen, R. D. Piner, L. Colombo, and R. S. Ruoff, "Transfer of Large-Area Graphene Films for High-Performance Transparent Conductive Electrodes," *Nano Lett*, **9**(12), 4359 (2009).
7. D. Li, M. B. Mueller, S. Gilje, R. B. Kaner, and G. G. Wallace, "Processable aqueous dispersions of graphene nanosheets," *Nat. Nanotechnol.*, **3**(2), 101 (2008).
8. S. Hu and X. Wang, "Ultrathin nanostructures: smaller size with new phenomena," *Chem. Soc. Rev.*, **42**(12), 5577 (2013).
9. B. Aufray, A. Kara, S. Vizzini, H. Oughaddou, C. Leandri, B. Ealet, and G. Le Lay, "Graphene-like silicon nanoribbons on Ag(110): A possible formation of silicene," *Applied Physics Letters*, **96**(18), 183102 (2010).
10. A. Kara, H. Enriquez, A. P. Seitsonen, L. C. L. Y. Voon, S. Vizzini, B. Aufray, and H. Oughaddou, "A review on silicene - New candidate for electronics," *Surface Science Reports*, **67**(1), 1 (2012).
11. A. O'Hare, F. V. Kusmartsev, and K. I. Kugel, "A Stable "Flat" Form of Two-Dimensional Crystals: Could Graphene, Silicene, Germanene Be Minigap Semiconductors?," *Nano Letters*, **12**(2), 1045 (2012).
12. S. Cahangirov, M. Topsakal, E. Akturk, H. Sahin, and S. Ciraci, "Two- and One-Dimensional Honeycomb Structures of Silicon and Germanium," *Phys. Rev. Lett.*, **102**(23), 236804/1 (2009).
13. F. Bechstedt, L. Matthes, P. Gori, and O. Pulci, "Infrared absorbance of silicene and germanene," *Applied Physics Letters*, **100**(26), 261906 (2012).
14. J. Wang, S. Deng, Z. Liu, and Z. Liu, "The rare two-dimensional materials with Dirac cones," *National Science Review*, **2**(1), 22 (2015).
15. Z. Ni, Q. Liu, K. Tang, J. Zheng, J. Zhou, R. Qin, Z. Gao, D. Yu, and J. Lu, "Tunable Bandgap in Silicene and Germanene," *Nano Letters*, **12**(1), 113 (2012).
16. Q. Pang, C. L. Zhang, L. Li, Z. Q. Fu, X. M. Wei, and Y. L. Song, "Adsorption of alkali metal atoms on germanene: A first-principles study," *Appl Surf Sci*, **314**, 15 (2014).
17. Y. Wang, Z. Ni, Q. Liu, R. Quhe, J. Zheng, M. Ye, D. Yu, J. Shi, J. Yang, J. Li, and J. Lu, "All-Metallic Vertical Transistors Based on Stacked Dirac Materials," *Adv. Funct. Mater.*, **25**(1), 68 (2015).
18. M. Derivaz, D. Dentel, R. Stephan, M.-C. Hanf, A. Mehdaoui, P. Sonnet, and C. Pirri, "Continuous germanene layer on Al(111)," *Nano Lett*, **15**(4), 2510 (2015).
19. M. Houssa, G. Pourtois, V. V. Afanas'ev, and A. Stesmans, "Electronic properties of two-dimensional hexagonal germanium," *Applied Physics Letters*, **96**(8), 082111 (2010).
20. W. Wei, Y. Dai, B. Huang, and T. Jacob, "Many-body effects in silicene, silicane, germanene and germanane," *Physical Chemistry Chemical Physics*, **15**(22), 8789 (2013).
21. D. Kaltsas and L. Tsetseris, "Stability and electronic properties of ultrathin films of silicon and germanium," *Physical Chemistry Chemical Physics*, **15**(24), 9710 (2013).
22. E. Scalise, M. Houssa, G. Pourtois, B. Broek, V. Afanas'ev, and A. Stesmans, "Vibrational properties of silicene and germanene," *Nano Res*, **6**(1), 19 (2013).
23. L. Matthes, O. Pulci, and F. Bechstedt, "Massive Dirac quasiparticles in the optical absorbance of graphene, silicene, germanene, and tinene," *Journal of Physics-Condensed Matter*, **25**(39), 395305 (2013).
24. N. J. Roome and J. D. Carey, "Beyond Graphene: Stable Elemental Monolayers of Silicene and Germanene," *ACS Appl. Mater. Interfaces*, **6**(10), 7743 (2014).
25. M. R. Tchalala, H. Enriquez, A. J. Mayne, A. Kara, G. Dujardin, M. A. Ali, and H. Oughaddou, "Iop Atomic structure of silicene nanoribbons on Ag(110)," *3rd International Meeting on Silicene (Ims-3)*, 491 (2014).
26. L. Li, S.-z. Lu, J. Pan, Z. Qin, Y.-q. Wang, Y. Wang, G.-y. Cao, S. Du, and H.-J. Gao, "Buckled Germanene Formation on Pt(111)," *Advanced Materials*, **26**(28), 4820 (2014).
27. M. E. Davila, L. Xian, S. Cahangirov, A. Rubio, and G. Le Lay, "Germanene: a novel two-dimensional germanium allotrope akin to graphene and silicene," *New J. Phys.*, **16** (Sept.), 095002/1, 10 pp (2014).
28. M. E. Davila and G. Le Lay, "Few layer epitaxial germanene: a novel two-dimensional Dirac material," *Sci. Rep.*, **6**, 20714 (2016).
29. P. Bampoulis, L. Zhang, A. Safaei, R. van Gastel, B. Poelsema, and H. J. W. Zandvliet, "Germanene termination of Ge$_2$Pt crystals on Ge(110)," *J. Phys.: Condens. Matter*, **26**(44), 442001/1 (2014).
30. H.-S. Tsai, Y.-Z. Chen, H. Medina, T.-Y. Su, T.-S. Chou, Y.-H. Chen, Y.-L. Chueh, and J.-H. Liang, "Direct formation of large-scale multi-layered germanene on Si substrate," *Phys. Chem. Chem. Phys.*, **17**(33), 21389 (2015).
31. F. d'Acapito, S. Torrengo, E. Xenogiannopoulou, P. Tsipas, J. M. Velasco, D. Tsoutsou, and A. Dimoulas, "Evidence for Germanene growth on epitaxial hexagonal (h)-AlN on Ag(111)," *Journal of Physics-Condensed Matter*, **28**(4) (2016).
32. E. Bianco, S. Butler, S. Jiang, O. D. Restrepo, W. Windl, and J. E. Goldberger, "Stability and Exfoliation of Germanane: A Germanium Graphane Analogue," *ACS Nano*, **7**(5), 4414 (2013).
33. S. Jayakrishnan, M. Pushpavanam, and B. A. Shenoi, "Electrodeposition from organic solutions of metals that are difficult to deposit from aqueous solutions," *Surf. Technol.*, **13**(3), 225 (1981).
34. G. Szekely, "Electrodeposition of germanium," *J. Electrochem. Soc.*, **98**, 318 (1951).
35. A. Lahiri, S. Zein El Abedin, and F. Endres, "UV-Assisted Electrodeposition of Germanium from an Air- and Water-Stable Ionic Liquid," *J. Phys. Chem. C*, **116**(33), 17739 (2012).
36. M. Wu, N. R. Brooks, S. Schaltin, K. Binnemans, and J. Fransaer, "Electrodeposition of germanium from the ionic liquid 1-butyl-1-methylpyrrolidinium dicyanamide," *Phys. Chem. Chem. Phys.*, **15**(14), 4955 (2013).
37. M. Wu, G. Vanhoutte, N. R. Brooks, K. Binnemans, and J. Fransaer, "Electrodeposition of germanium at elevated temperatures and pressures from ionic liquids," *Phys. Chem. Chem. Phys.*, **17**(18), 12080 (2015).
38. F. Endres and C. Schrodt, "*In situ* STM studies on germanium tetraiodide electroreduction on Au(111) in the room temperature molten salt 1-butyl-3-methylimidazolium hexafluorophosphate," *Phys. Chem. Chem. Phys.*, **2**(24), 5517 (2000).
39. F. Endres, "Electrodeposition of a thin germanium film on gold from a room temperature ionic liquid," *Phys. Chem. Chem. Phys.*, **3**(15), 3165 (2001).
40. F. Endres, "Electrodeposition of nanosized germanium from GeBr$_4$ and GeCl$_4$ in an ionic liquid," *Electrochem. Solid-State Lett.*, **5**(3), C38 (2002).
41. F. Endres and S. Zein El Abedin, "Nanoscale electrodeposition of germanium on Au(111) from an ionic liquid: an in situ STM study of phase formation. Part II. Ge from GeCl$_4$," *Phys. Chem. Chem. Phys.*, **4**(9), 1649 (2002).
42. F. Endres and S. Zein El Abedin, Nanoscale electrodeposition of germanium on Au(111) from an ionic liquid: an in situ STM study of phase formation. Part I. Ge from GeBr$_4$," *Phys. Chem. Chem. Phys.*, **4**(9), 1640 (2002).
43. I. Mukhopadhyay and W. Freyland, "Thickness induced metal-nonmetal transition in ultrathin electrodeposited Ge films," *Chem. Phys. Lett.*, **377**(1,2), 223 (2003).
44. R. Al-Salman, J. Mallet, M. Molinari, P. Fricoteaux, F. Martineau, M. Troyon, Z. S. El Abedin, and F. Endres, "Template assisted electrodeposition of germanium and silicon nanowires in an ionic liquid," *Phys. Chem. Chem. Phys.*, **10**(41), 6233 (2008).
45. M. J. Jawad, M. R. Hashim, N. K. Ali, E. P. Corcoles, and M. E. Sharifabad, "An Alternative Method to Grow Ge Thin Films on Si by Electrochemical Deposition for Photonic Applications," *J. Electrochem. Soc.*, **159**(2), D124 (2012).
46. J. Ke, P. N. Bartlett, D. Cook, T. L. Easun, M. W. George, W. Levason, G. Reid, D. Smith, W. T. Su, and W. J. Zhang, "Electrodeposition of germanium from supercritical fluids," *Physical Chemistry Chemical Physics*, **14**(4), 1517 (2012).
47. Q. Huang, S. W. Bedell, K. L. Saenger, M. Copel, H. Deligianni, and L. T. Romankiw, "Single-crystalline germanium thin films by electrodeposition and solid-phase epitaxy," *Electrochemical and Solid State Letters*, **10**(11), D124 (2007).
48. E. Fahrenkrug, J. Gu, S. Jeon, P. A. Veneman, R. S. Goldman, and S. Maldonado, "Room-Temperature Epitaxial Electrodeposition of Single-Crystalline Germanium Nanowires at the Wafer Scale from an Aqueous Solution," *Nano Lett*, **14**(2), 847 (2014).
49. N. K. Mahenderkar, Y.-C. Liu, J. A. Koza, and J. A. Switzer, "Electrodeposited germanium nanowires," *ACS Nano*, **8**(9), 9524 (2014).
50. A. I. Carim, S. M. Collins, J. M. Foley, and S. Maldonado, "Benchtop Electrochemical Liquid-Liquid-Solid Growth of Nanostructured Crystalline Germanium," *J. Am. Chem. Soc.*, **133**(34), 13292 (2011).
51. X. Liang, N. Jayaraju, C. Thambidurai, Q. Zhang, and J. L. Stickney, "Controlled Electrochemical Formation of Ge$_x$Sb$_y$Te$_z$ using Atomic Layer Deposition (ALD)," *Chem. Mater.*, **23**(7), 1742 (2011).
52. X. Liang, Y.-G. Kim, D. K. Gebergziabiher, and J. L. Stickney, "Aqueous Electrodeposition of Ge Monolayers," *Langmuir*, **26**(4), 2877 (2010).
53. X. Liang, Q. Zhang, M. D. Lay, and J. L. Stickney, "Growth of Ge Nanofilms Using Electrochemical Atomic Layer Deposition, with a "Bait and Switch" Surface-Limited Reaction," *J. Am. Chem. Soc.*, **133**(21), 8199 (2011).
54. J. Clavilier, R. Faure, G. Guinet, and R. Durand, "Preparation of monocrystalline platinum microelectrodes and electrochemical study of the plane surfaces cut in the direction of the {111} and {110} planes," *J. Electroanal. Chem. Interfacial Electrochem*, **107**(1), 205 (1980).
55. M. L. Foresti, A. Pozzi, M. Innocenti, G. Pezzatini, F. Loglio, E. Salvietti, A. Giusti, F. D'Anca, R. Felici, and F. Borgatti, "In situ X-ray analysis under controlled potential

conditions: An innovative setup and its application to the investigation of ultrathin films electrodeposited on Ag(111)," *Electrochimica Acta*, **51**(25), 5532 (2006).

56. S. Roobol, W. Onderwaater, J. Drnec, R. Felici, and J. Frenken, "BINoculars: data reduction and analysis software for two-dimensional detectors in surface X-ray diffraction," *J Appl Crystallogr*, **48**, 1324 (2015).

57. J. Drnec, T. Zhou, S. Pintea, W. Onderwaater, E. Vlieg, G. Renaud, and R. Felici, "Integration techniques for surface X-ray diffraction data obtained with a two-dimensional detector," *J Appl Crystallogr*, **47**, 365 (2014).

58. E. Vlieg, "ROD: A program for surface X-ray crystallography," *J Appl Crystallogr*, **33**, 401 (2000).

59. J. Wang, B. M. Ocko, A. J. Davenport, and H. S. Isaacs, "*In situ* X-Ray-Diffraction and X-Ray-Reflectivity Studies of the Au(111) Electrolyte Interface - Reconstruction and Anion Adsorption," *Physical Review B*, **46**(16), 10321 (1992).

60. A. R. Sandy, S. G. J. Mochrie, D. M. Zehner, K. G. Huang, and D. Gibbs, "Structure and Phases of the Au(111) Surface - X-Ray-Scattering Measurements," *Physical Review B*, **43**(6), 4667 (1991).

61. P. Allongue, L. Cagnon, C. Gomes, A. Gundel, and V. Costa, "Electrodeposition of Co and Ni/Au(111) ultrathin layers. Part I: nucleation and growth mechanisms from in situ STM," *Surface Science*, **557**(1-3), 41 (2004).

62. Y. Nahas, V. Repain, C. Chacon, Y. Girard, and S. Rousset, "Interplay between ordered growth and intermixing of Pt on patterned Au surfaces," *Surf. Sci.*, **604**(9-10), 829 (2010).

63. P. Campiglio, V. Repain, C. Chacon, O. Fruchart, J. Lagoute, Y. Girard, and S. Rousset, "Quasi unidimensional growth of Co nanostructures on a strained Au(111) surface," *Surf. Sci.*, **605**(13-14), 1165 (2011).

64. F. Besenbacher, J. V. Lauritsen, T. R. Linderoth, E. Laegsgaard, R. T. Vang, and S. Wendt, "Atomic-scale surface science phenomena studied by scanning tunneling microscopy," *Surface Science*, **603**(10-12), 1315 (2009).

65. A. E. Baber, H. L. Tierney, and E. C. H. Sykes, "Atomic-Scale Geometry and Electronic Structure of Catalytically Important Pd/Au Alloys," *ACS Nano*, **4**(3), 1637 (2010).

66. J. T. Sun, L. Gao, X. B. He, Z. H. Cheng, Z. T. Deng, X. Lin, H. Hu, S. X. Du, F. Liu, and H. J. Gao, "Surface reconstruction transition of metals induced by molecular adsorption," *Phys. Rev. B: Condens. Matter Mater. Phys.*, **83**(11), 115419/1 (2011).

67. C. Polop, C. Rojas, J. A. Martin-Gago, R. Fasel, J. Hayoz, D. Naumovic, and P. Aebi, "Structure of Si atomic chains grown on the Si/Cu(110) c(2 × 2) surface alloy," *Phys. Rev. B: Condens. Matter Mater. Phys.*, **63**(11), 115414/1 (2001).

68. P. De Padova, C. Quaresima, P. Perfetti, B. Olivieri, C. Leandri, B. Aufray, S. Vizzini, and G. Le Lay, "Growth of Straight, Atomically Perfect, Highly Metallic Silicon Nanowires with Chiral Asymmetry," *Nano Lett*, **8**(1), 271 (2008).

69. A. Kara, C. Leandri, M. E. Davila, P. Padova, B. Ealet, H. Oughaddou, B. Aufray, and G. Lay, "Physics of Silicene Stripes," *J. Supercond. Novel Magn.*, **22**(3), 259 (2009).

70. G. Le Lay, B. Aufray, C. Leandri, H. Oughaddou, J. P. Biberian, P. De Padova, M. E. Davila, B. Ealet, and A. Kara, "Physics and chemistry of silicene nano-ribbons," *Appl Surf Sci*, **256**(2), 524 (2009).

71. B. Aufray, A. Kara, S. Vizzini, H. Oughaddou, C. Leandri, B. Ealet, and G. Le Lay, "Graphene-like silicon nanoribbons on Ag(110). A possible formation of silicene," *Appl. Phys. Lett.*, **96**(18), 183102/1 (2010).

72. P. De Padova, C. Quaresima, C. Ottaviani, P. M. Sheverdyaeva, P. Moras, C. Carbone, D. Topwal, B. Olivieri, A. Kara, H. Oughaddou, B. Aufray, and G. Le Lay, "Evidence of graphene-like electronic signature in silicene nanoribbons," *Appl. Phys. Lett.*, **96**(26), 261905/1-261905/3 (2010).

73. F. Ronci, S. Colonna, A. Cricenti, P. De Padova, C. Ottaviani, C. Quaresima, B. Aufray, and G. Le Lay, "Low temperature STM/STS study of silicon nanowires grown on the Ag(110) surface," *Phys. Status Solidi C*, **7**(11-12), 2716 (2010).

74. P. De Padova, P. Perfetti, B. Olivieri, C. Quaresima, C. Ottaviani, and G. Le Lay, "1D graphene-like silicon systems: silicene nano-ribbons" *J. Phys.: Condens. Matter*, **24**(22), 223001/1 (2012).

75. N. T. M. Hai, M. Van der Auweraer, K. Mullen, and S. De Feyter, "Self-Assembly of a Functionalized Alkylated Isophthalic Acid at the Au(111)/Electrolyte Interface: Structure and Dynamics," *J Phys Chem C*, **113**(27), 11567 (2009).

76. F. Endres, "The electrodeposition of germanium from an ionic liquid: A mini-review on the nanoscale processes," *Proc. - Electrochem. Soc.*, **2002–19**(Molten Salts XIII), 677 (2002).

77. F. Endres and Z. S. El Abedin, "Nanoscale electrodeposition of germanium on Au(111) from an ionic liquid: an in situ STM study of phase formation - Part I. Ge from GeBr4," *Physical Chemistry Chemical Physics*, **4**(9), 1640 (2002).

78. P. M. Ajayan and B. I. Yakobson, "Graphene. Pushing the boundaries," *Nat. Mater.*, **10**(6), 415 (2011).

79. P. Y. Huang, C. S. Ruiz-Vargas, A. M. van der Zande, W. S. Whitney, M. P. Levendorf, J. W. Kevek, S. Garg, J. S. Alden, C. J. Hustedt, Y. Zhu, J. Park, P. L. McEuen, and D. A. Muller, "Grains and grain boundaries in single-layer graphene atomic patchwork quilts," *Nature (London, U. K.)*, **469**(7330), 389 (2011).

80. P. T. Araujo, M. Terrones, and M. S. Dresselhaus, "Defects and impurities in graphene-like materials," *Mater. Today (Oxford, U. K.)*, **15**(3), 98 (2012).

81. L. Sun, F. Banhart, and J. Warner, "Two-dimensional materials under electron irradiation," *MRS Bull*, **40**(1), 29 (2015).

82. A. I. Carim, J. Gu, and S. Maldonado, "Overlayer Surface-Enhanced Raman Spectroscopy for Studying the Electrodeposition and Interfacial Chemistry of Ultrathin Ge on a Nanostructured Support," *ACS Nano*, **5**(3), 1818 (2011).